

Turbulent Dynamics and Heat Transfer in Transcritical Channel Flow

Kukjin Kim

School of Mechanical Engineering
Purdue University
585 Purdue Mall, West Lafayette, IN 47907, USA
kim1625@purdue.edu

Carlo Scalo

School of Mechanical Engineering
Purdue University
585 Purdue Mall, West Lafayette, IN 47907, USA
scalo@purdue.edu

Jean-Pierre Hickey

Department of Mechanical and Mechatronics Engineering
University of Waterloo
200 University Avenue West, Waterloo, ON N2L 3G1, Canada
jean-pierre.hickey@uwaterloo.ca

ABSTRACT

We present direct numerical simulations (DNS) of turbulent channel flow to study turbulent dynamics and heat transfer effects at a transcritical temperature and supercritical pressure regime. The fully compressible Navier–Stokes equations in conservative form are closed with the Peng–Robinson (PR) equation of state and the Chung’s model for the thermophysical and transport properties. To quantify the turbulent heat transfer effect, the bottom and top walls of the channel are maintained at different isothermal temperatures, $T_{top/bot} = T_{pb} \pm \Delta T/2$, where T_{pb} is the pseudoboiling temperature of working fluid and $\Delta T = 20$ K. The bulk pressure and velocity are $1.1p_c$ and 36 m/s, respectively, where p_c is the critical pressure.

The statistical mean profiles shows significant thermophysical variation in the regime having large thermodynamic gradient near the walls compared to the ideal gas case and the average pseudoboiling location is observed at $y/h = 0.92$. The root mean square (RMS) profiles of fluctuating velocity are attenuated in the pseudogas region, whereas the thermodynamic fluctuations are greater in that region than the pseudoliquid region. One-dimensional energy spectra fall off steeply at high wavenumber showing the adequacy of the DNS resolution. Instantaneous visualizations of near-wall turbulent structures reveal that the dense fluid ejection from the bottom wall reaches to the channel center region resulting in the large fluctuation in the thermodynamic properties across the channel.

INTRODUCTION

Gas turbine and liquid rocket engines operate under increasingly higher temperatures and pressures. These extreme thermodynamic conditions often exceed the critical point and a near-critical fluid around the point has peculiar thermophysical features such as liquid-like density, gas-like diffusivity, and zero surface tension making a clear distinction between the liquid and gas phase difficult (Yang, 2000).

Studies of heat transfer and thermodynamic characteristics at such environment have been conducted in channel or pipe flows. Pizzarelli *et al.* (2009) investigated the turbulent channel flow considering real fluid effects at supercritical pressure and it was indicated that temperature diffusion is less intense across the channel because the thermal diffusivity of real fluids is lower than that of ideal gas, therefore, showing different temperature stratification between them and reduction of turbulent kinetic energy (TKE) has an effect on heat transfer deterioration. Nemati *et al.* (2015) carried out DNS of heated pipe flows at supercritical pressure regime and

confirmed that thermal expansion resulted from the wall heat flux reduces the TKE significantly with small buoyancy effect, however, high buoyancy causes the increase of turbulence intensity. Wang *et al.* (2010) showed that heat transfer in the channel flow is improved by increasing of inlet pressure with cryogenic propellant and the heat transfer and pressure loss are affected by the aspect ratio variation in the channel cross-section. Patel *et al.* (2015) investigated the effects of different combinations of density and viscosity and confirmed that the statistic results of the heated turbulent channel flow show quasi-similarity with constant semi-local Reynolds number, and therefore, the modulation technique in turbulence can be applied to the turbulent flow with heat transfer. Kawai (2016) studied the characteristics of the turbulent boundary layers (TBL) affected by the real fluid effects in unheated and heated flat plate flows. The strong compressibility in the heated flow caused density fluctuation in the TBL transcritical region so that turbulent diffusion, pressure dilatation, and mass flux respond to the fluctuation.

In this study, we have carried out direct numerical simulations (DNS) of a canonical channel flow setup to characterize the turbulent flow dynamics and transcritical heat transfer effects. In the following, we explain the governing equations with computational setup conditions and the statistical studies and instantaneous turbulent structures are investigated.

PROBLEM FORMULATION

The fully compressible Navier–Stokes equations in conservative form are solved with a high order compact finite difference scheme (Larsson & Lele, 2009) and are as follows,

$$\frac{\partial \rho}{\partial t} + \frac{\partial \rho u_j}{\partial x_j} = 0 \quad (1)$$

$$\frac{\partial \rho u_i}{\partial t} + \frac{\partial \rho u_i u_j}{\partial x_j} = -\frac{\partial p}{\partial x_i} + \frac{\partial \tau_{ij}}{\partial x_j} \quad (2)$$

$$\frac{\partial \rho E}{\partial t} + \frac{\partial [u_j (\rho E + p)]}{\partial x_j} = \frac{\partial (u_i \tau_{ij} - q_j)}{\partial x_j} \quad (3)$$

where x_i and u_i are coordinate and velocity component, respectively. ρ is the density, p the pressure, E the total energy per unit mass, τ_{ij} the viscous flux, and q_j the conductive heat flux.

To model the thermodynamic properties considering real fluid effects, the Peng–Robinson (PR) equation of state (Peng & Robinson, 1976) and the departure functions (Sengers *et al.*, 2000) are

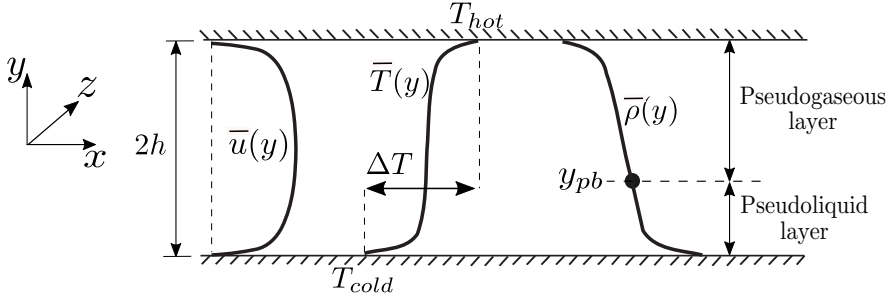


Figure 1: Physical setup (left) and the phase diagram showing the specific heat capacity isolines (—), the critical point (●), and the pseudoboiling line (- - -) of R-134a (right).

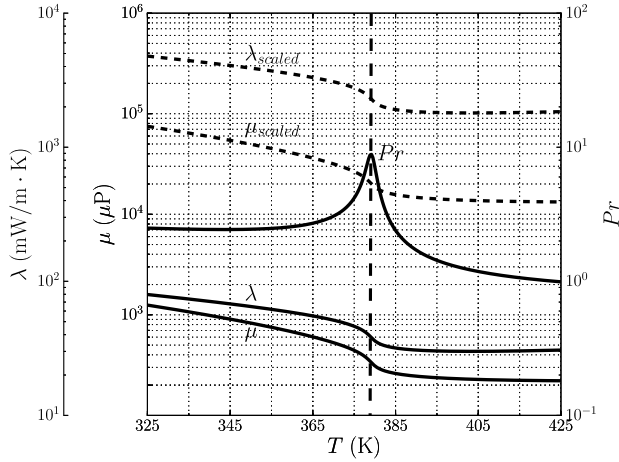


Figure 2: Transport properties computed by the Chung's model (—) and their augmented profiles used in the computation (- - -).

used.

$$p = \frac{R_u T}{v_m - b} - \frac{a\alpha}{v_m^2 + 2bv_m - b^2} \quad (4)$$

where R_u is the universal gas constant, T the temperature, and v_m the molar volume. a , b , and α represent attractive and repulsive effects between molecules and nonspherical characteristic of molecule. Also, the Chung's model is used to compute transport properties. All the details are shown in Chung *et al.* (1984, 1988).

The physical setup is a canonical compressible turbulent channel flow with isothermal top and bottom wall temperature conditions, $T_{top/bot} = T_{pb} \pm \Delta T/2$, where T_{pb} is the pseudoboiling temperature of working fluid, R-134a. The pseudoboiling point is defined as the locus having local maximum heat capacity at given supercritical pressure condition and the pseudoboiling line (PBL) is the line connecting the points (see figure 1). The bulk pressure, $p_b = 1.1p_c$ resulting in $T_{pb} = 379.1$ K for R-134a. In this study, the wall temperature difference constructing the transcritical temperature condition, $\Delta T = 20$ K and it brackets T_{pb} . The bulk density and streamwise velocity are 520 kg/m^3 and 36 m/s and other details are shown in table 1.

Since the DNS requires the resolution of all the relevant turbulent scales of the flow, the friction velocity near the wall is the

Table 1: Computational parameters.

Fluid	R-134a (CH_2FCF_3)
p_b	44.649 bar ($1.1p_c$)
T_{pb}	379.1 K
ΔT	20 K (369.1–389.1)
ρ_b	520 kg/m^3
L_x, L_y, L_z	12, 2, 4 mm
U_b	36 m/s

key to make the DNS feasible. The friction Reynolds number, $Re_\tau = hu_\tau/\nu$ where h is the channel half-width, u_{tau} the friction velocity, and ν the kinematic viscosity, is set at the specific balanced range in terms of an efficient computation and physical validity. In this study, we have selected the scaling factor with 60 to augment viscosity and thermal conductivity resulting in $Re_\tau = 375$ and maintaining a physical Prandtl number. Also, the nondimensional ideal gas case is considered as a reference with $p_b = 0.71$, $\rho_b = 1.0$, $U_b = 0.26$, $T_{pb} = 1.0$, $\Delta T = 0.4$, $T_{bot} = 0.8$, $T_{top} = 1.2$, and $8 \times 2 \times 4$ for the box size.

RESULTS AND DISCUSSION

Statistical Study

In the following, the mean and RMS statistics are analyzed and compared against the equivalent ideal gas case with the grid resolution on the one-dimensional energy spectra.

Time averaged density, temperature, and compressibility factor profiles are shown in figure 3. The mean density profile using the real fluid model results in a significantly increased top-to-bottom difference compared to the ideal gas profile based on $\Delta T = 20$ K; $\rho_{real} = 274.2\text{--}722.6 \text{ kg/m}^3$, $\rho_{ideal} = 433.9\text{--}647.4 \text{ kg/m}^3$. Departure from the ideal gas behavior is also seen from the compressibility factor. Especially, the compressibility factor value on the top wall is approximately half of the value corresponding to the ideal gas condition and the pseudoliquid state at the bottom wall exhibits even greater departure from the ideal gas behavior ($Z_{real} = 0.20\text{--}0.51$). The average pseudoboiling location is located near the top wall (at $y/h = 0.92$) meaning that most of the channel flow is characterized by the pseudoliquid flow and thermodynamic variations is

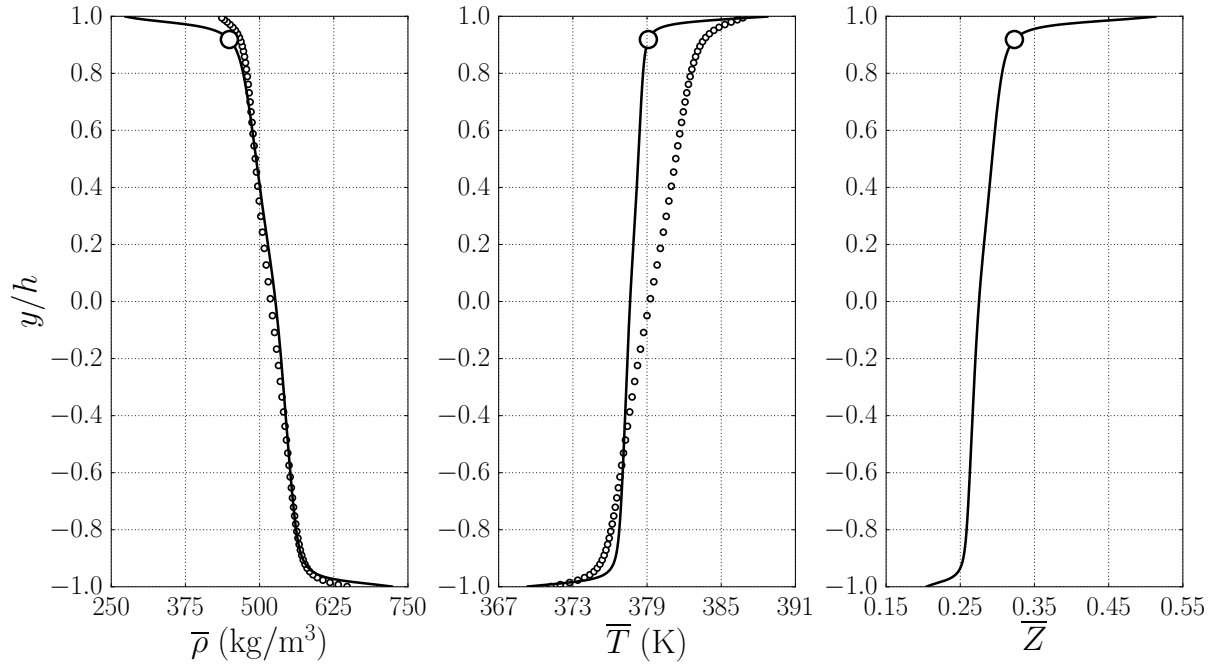


Figure 3: Statistical mean profiles (—) of density (left), temperature (middle), and compressibility factor (right) with the average pseudoboiling location (○) and the ideal gas data (○).

more pronounced near the top wall, and therefore the dependence of wall-bounded turbulence effect on the thermodynamic fluctuations will grow. Also, large gradient in those mean quantities is observed within the ranges of $y/h = -1.0$ – -0.9 (bottom wall region) and 0.9 – 1.0 (top wall region), which results in intense thermodynamic fluctuations.

Favre averaged hydrodynamic and thermodynamic fluctuating quantities are shown in figures 4 and 5. The RMS profiles of the velocity fluctuation in figure 4 have two local peaks in the near-wall regions which are expected given the large velocity gradients. The RMS peaks near the top wall have lower values than those observed in the bottom wall; u''_{RMS} , v''_{RMS} , and w''_{RMS} in the pseudogaseous flow decrease 4.15 %, 21.31 %, and 18.48 %, respectively, compared to the pseudoliquid flow. Also, the ideal gas case has the typical symmetric RMS profiles in its hydrodynamics, whereas the real fluid effect and the biased location of pseudoboiling cause attenuation in the top near-wall region within $y/h = 0.1$ – 0.9 .

On the other hand, the profiles of thermodynamic fluctuations shown in figure 5 have different aspects from the hydrodynamic quantities. The RMS profiles of density and temperature have peaks in both near-wall regions which are similar to those observed in the hydrodynamic fluctuating quantities. However, a marked difference is that the fluctuation intensity becomes stronger in the pseudogaseous region compared to the pseudoliquid region. Consequently, the transversal pseudoboiling line near the top wall leads to the intensification of the thermodynamic fluctuations in this region. The T''_{RMS} profile for the ideal gas case, as well as the real fluid one, shows a slight third peak along the centerline. The relative temperature fluctuation intensity at the third peak in the ideal gas flow is stronger than the real fluid case, however, the density fluctuation RMS of real fluid is higher than the ideal gas; $\rho''_{RMS,ideal} = 15.64 \text{ kg/m}^3$ and $\rho''_{RMS,real} = 20.06 \text{ kg/m}^3$ at the third peak. This phenomenon corresponds to the rapid variance in the mean density profile with small change in temperature (see figure 3) and therefore leads significant momentum fluctuation across the channel. Also, the third peak location moves towards the top near-wall region (at $y/h = 0.22$) com-

pared to the ideal gas case observed in the centerline and this makes the wall-bounded turbulent flow more biased. Meanwhile, the pressure fluctuating intensity of real fluid is weaker than the ideal gas across the channel and it has less effect on the density variation than temperature.

Figure 6 shows one-dimensional energy spectra of fluctuating density and temperature at the two near-wall peaks of density fluctuation RMS and the centerplane. All the profiles fall off steeply at high wavenumber that is a general tendency in the turbulent flows and verifies the adequacy of all the DNS resolutions. Even though the governing equations in conservative form show build-up at high wavenumber in the energy spectra, this was mitigated by a high numerical resolution for the given Reynolds number.

To investigate distribution of the thermodynamic fluctuations, the probability density functions (PDF) of density and its fluctuation are shown in figure 7. The density PDF contour reflects well the mean density profile in figure 3 (significant difference between the walls and large gradient near the walls) and has the maximum probability at the walls since the density distribution at the walls is dominated by the isothermal wall conditions. The fluctuating density PDF at $y/h = \pm 1.0$ shows the narrow fluctuation range and the steep profiles supporting the tendency observed in the PDF contour. On the other hand, the profile at the centerline has the biased shape which is the wide-negative and narrow-positive fluctuation and it is intensified at the average pseudoboiling location. This greater spread can be caused by the top near-wall turbulent activity.

Instantaneous Visualization

Figure 8 shows the instantaneous visualizations of the bottom near-wall turbulent structure and heat transfer. The density isosurface exhibits a clear ejection behavior in the pseudoliquid region. The near-wall turbulent structures eject the dense fluid into the less dense core of the channel and the turbulent structures shown in the Q-criterion follow the mainstream of ejected dense flow. Also, as the ejected flow has large inertia, it reaches to the center region

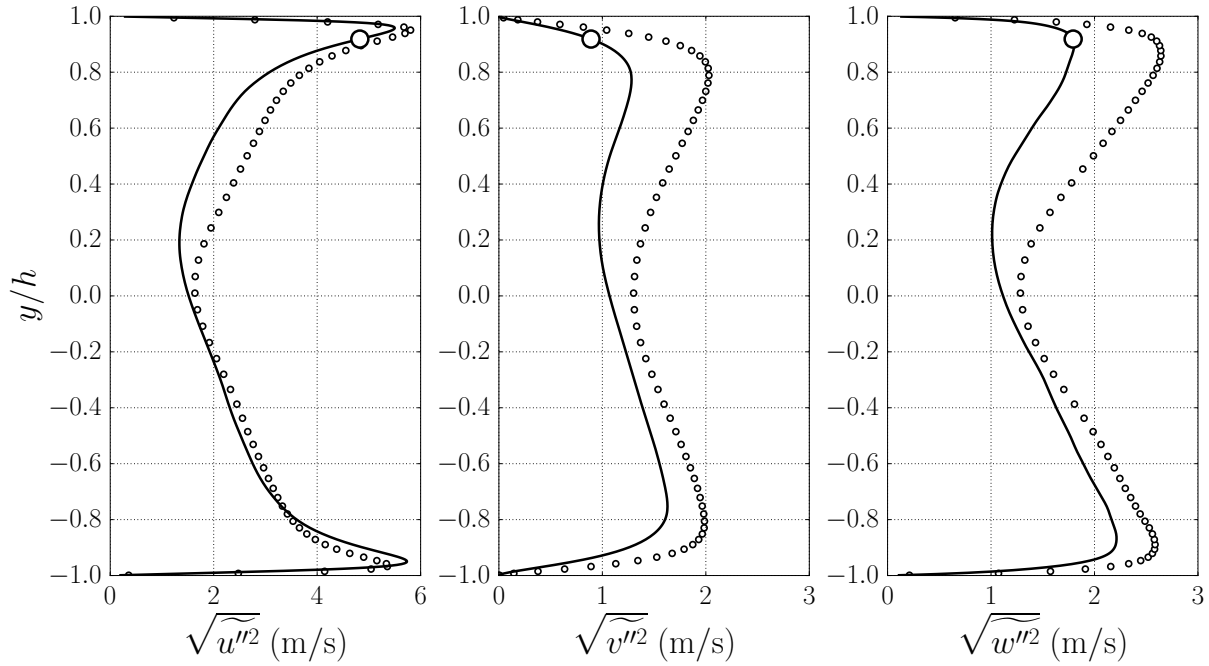


Figure 4: Statistical RMS profiles (—) of fluctuating velocity in the streamwise (left), wall-normal (middle), and spanwise (right) direction with the average pseudoboiling location (\circ) and the ideal gas data (\circ).

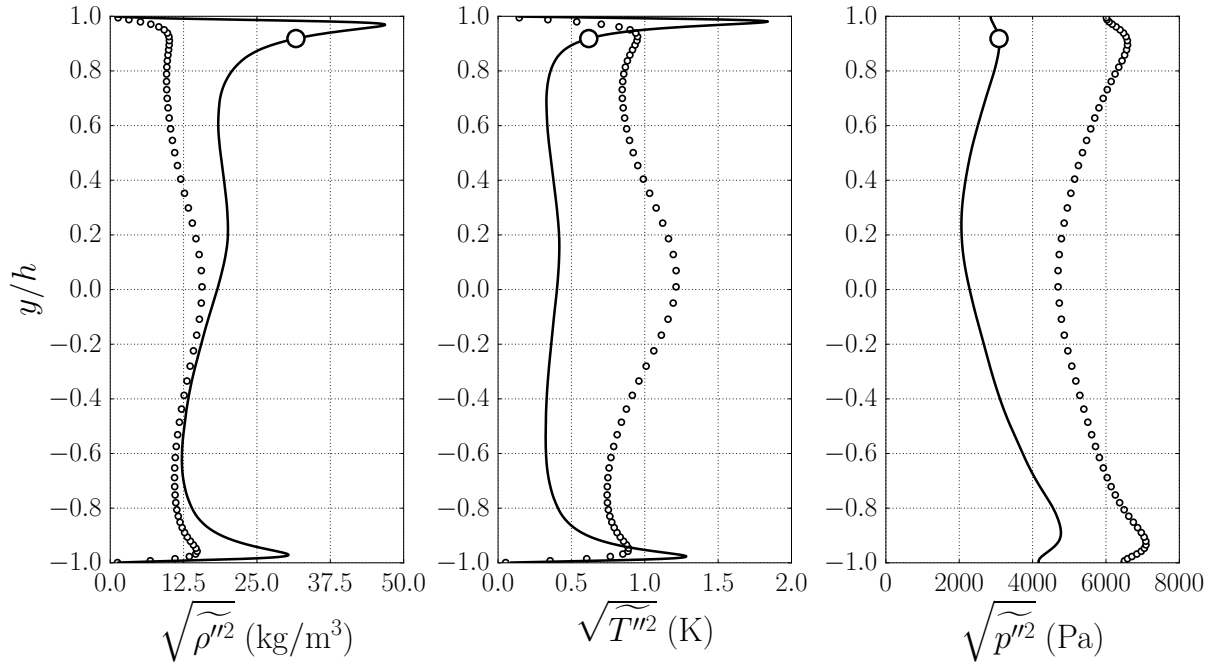


Figure 5: Statistical RMS profiles (—) of fluctuating density (left), temperature (middle), and pressure (right) with the average pseudoboiling location (\circ) and the ideal gas data (\circ).

of the channel where the fluid particles undergo a pseudotransition. This has concomitant effects on the thermodynamics which is a unique characteristics in the transcritical temperature regime and the temperature gradient isosurface exhibits streaks in black and those thermal traces are formed by the pseudoliquid flow structure.

CONCLUSIONS

We have performed direct numerical simulations (DNS) of transcritical turbulent channel flow with differentially heated walls ($T_{top} - T_{bot} = \Delta T$) of R-134a at a slightly supercritical pressure. The simulation were conducted by solving the fully compressible Navier–Stokes equations with conservative formulation. The PR equation of state was used with a consistent thermodynamic formulation to predict real fluid effects. A realistic Prandtl number is used

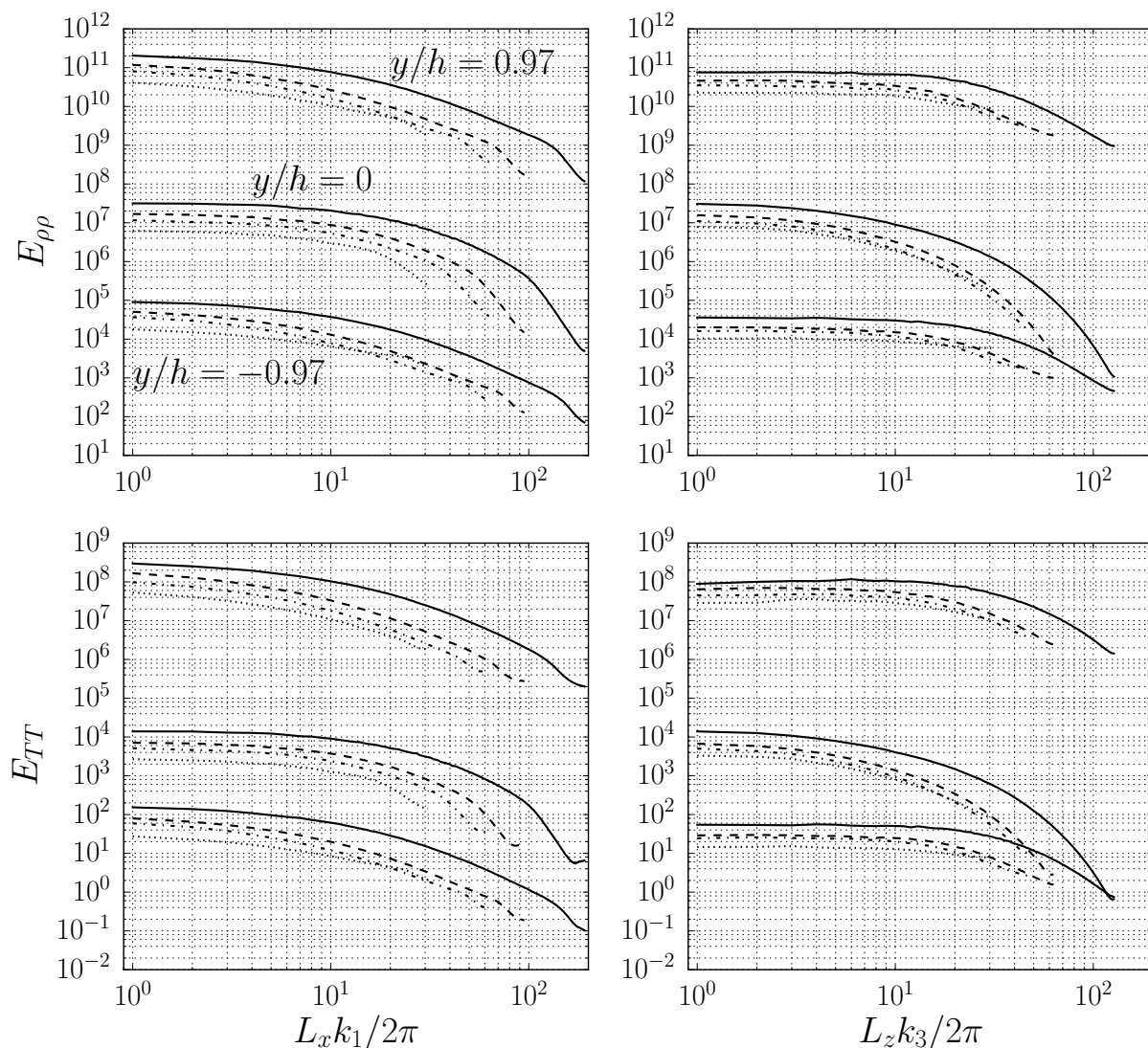


Figure 6: One-dimensional energy spectra of fluctuating density (top) and temperature (bottom) in the streamwise (left) and spanwise (right) direction extracted at $y/h = 0, \pm 0.97$ and grid resolution of $64 \times 96 \times 64$ (\cdots), $128 \times 128 \times 96$ ($-\cdot-$), $192 \times 128 \times 128$ ($- - -$), and $384 \times 256 \times 256$ ($—$). Spectra have been shifted by 3 decades for the centerline data and 6 decades for the top near-wall data.

and taken from the Chung's model to estimate the thermal conductivity.

The mean quantity profiles reveal that average pseudoboiling location is located at $y/h = 0.92$ and the density on the bottom wall equals 2.64 times that on the top wall so that shows huge disparity from the ideal gas which is in variation of $\rho_{ideal} = 433.9\text{--}647.4 \text{ kg/m}^3$, at equivalent pressure and temperature conditions. The well-known dual peaks in the turbulence quantities are located at $y/h = \pm 0.97$. The hydrodynamic velocity fluctuations are attenuated, while the thermodynamic fluctuation quantities for density and temperature have shown stronger intensity in the pseudogas region compared to the pseudoliquid region. The one-dimensional energy spectra support the robustness of these DNS calculations. The PDF contour and profile have shown that the strong thermodynamic fluctuation is caused by the wall-bounded turbulence near the top wall. Also, it is confirmed that the strong ejections of heavy fluid into the channel core affect the structures and dynamics of turbulent channel flow and leave the heat transfer streaks at the wall.

REFERENCES

- Chung, T.-H., Ajlan, M., Lee, L. L. & Starling, K. E. 1988 Generalized multiparameter correlation for nonpolar and polar fluid transport properties. *Industrial & Engineering Chemistry Fundamentals* **27** (4), 671–679.
- Chung, T.-H., Lee, L. L. & Starling, K. E. 1984 Applications of kinetic gas theories and multiparameter correlation for prediction of dilute gas viscosity and thermal conductivity. *Industrial & Engineering Chemistry Fundamentals* **23** (1), 8–13.
- Kawai, S. 2016 Direct numerical simulation of transcritical turbulent boundary layers at supercritical pressures with strong real fluid effects. In *54th AIAA Aerospace Sciences Meeting*, p. 1992. San Diego, CA: AIAA.
- Larsson, J. & Lele, S. K. 2009 Direct numerical simulation of canonical shock/turbulence interaction. *Phys. Fluids* **21**, 126101.
- Nemati, H., Patel, A., Boersma, B. J. & Pecnik, R. 2015 Mean statistics of a heated turbulent pipe flow at supercritical pressure. *International Journal of Heat and Mass Transfer* **83**, 741–752.
- Patel, A., Peeters, J. W. R., Boersma, B. J. & Pecnik, R. 2015 Semi-

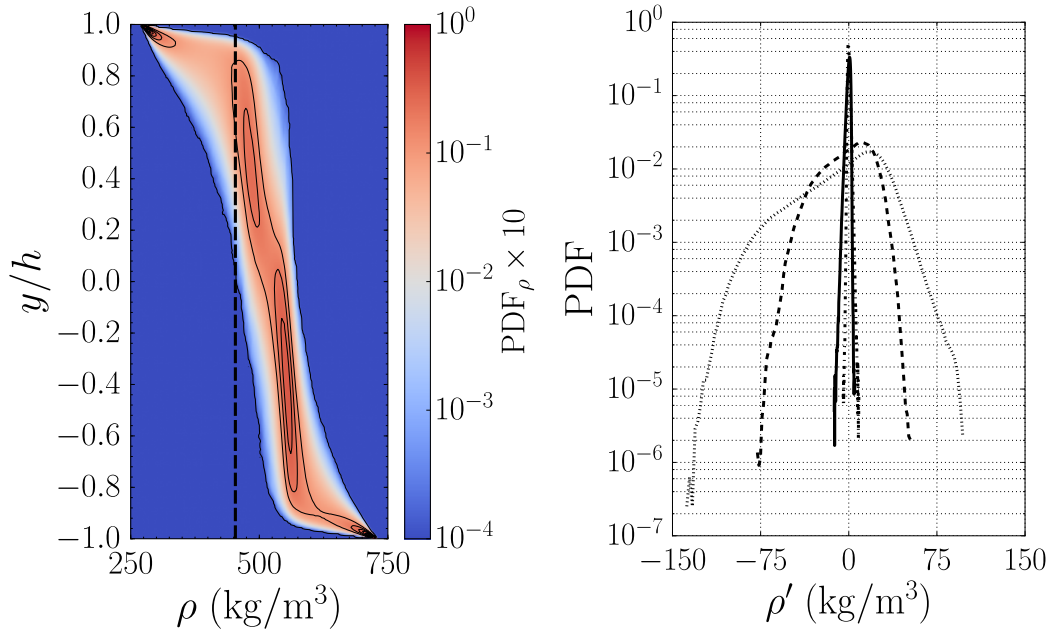


Figure 7: Density PDF contour (left) with the average pseudoboiling location (—) and fluctuating density PDF (right) at $y/h = -1.0$ (—), 0.0 (- - -), 1.0 (- · -), and y_{pb}/h (···).

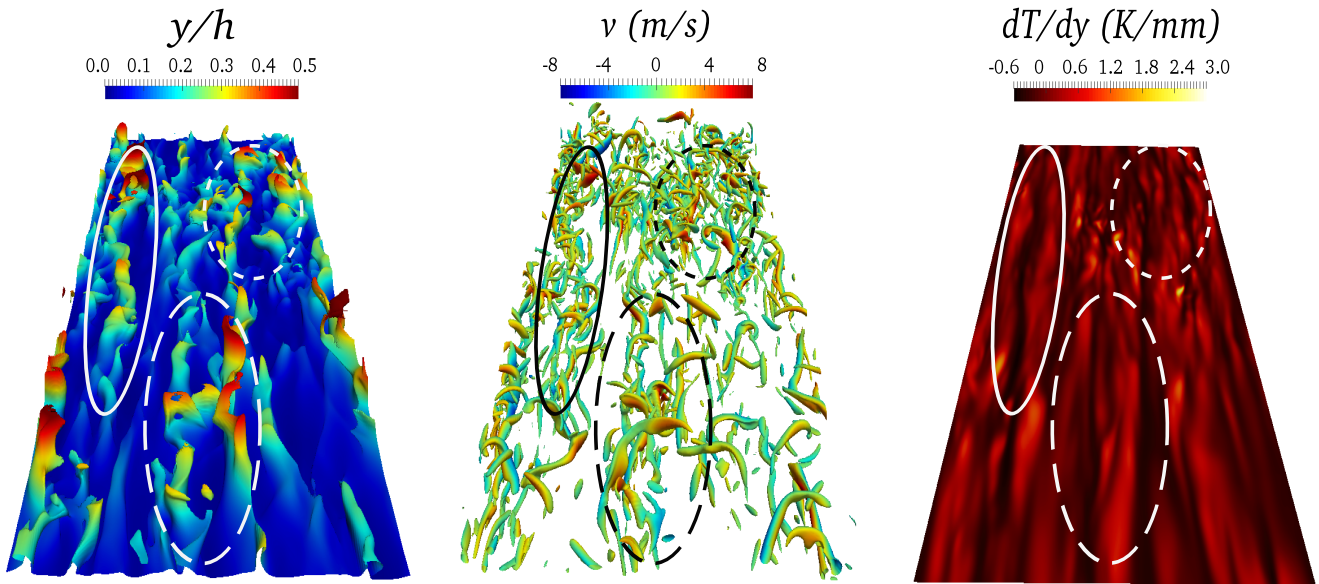


Figure 8: Isosurfaces of density ($\rho = 580 \text{ kg/m}^3$) colored by the distance from the bottom wall (left), Q-criterion ($Q = 2 \times 10^9 \text{ 1/s}^2$) colored by the wall-normal velocity (middle), and temperature gradient (right).

local scaling and turbulence modulation in variable property turbulent channel flows. *Physics of Fluids* **27**, 095101.

Peng, D.-Y. & Robinson, D. B. 1976 A new two-constant equation of state. *Industrial & Engineering Chemistry Fundamentals* **15** (1), 59–64.

Pizzarelli, M., Nasuti, F., Paciorni, R. & Onofri, M. 2009 Numerical analysis of three-dimensional flow of supercritical fluid in asymmetrically heated channels. *AIAA Journal* **47** (11), 2534–2543.

Sengers, J. V., Kayser, R. F., Peters, C. J., H. J. White, Jr., Ewing, M. B., Trusler, J. P. M., Anderko, A., Boublik, T., Kalyuzhnyi, Yu. V., Cummings, P. T., Smirnova, N. A., Victorov, A. V., Ely,

J. F., Marrucho, I. M. F., Sandler, S. I., Orbey, H., Matteoli, E., Hamad, E. Z., Mansoori, G. A. & Anisimov, M. A. 2000 *Equation of state for fluids and fluid mixtures. Part I*, 1st edn. Elsevier.

Wang, Y.-Z., Hua, Y.-X. & Meng, H. 2010 Numerical studies of supercritical turbulent convective heat transfer of cryogenic-propellant methane. *Journal of Thermophysics and Heat Transfer* **24** (3), 490–500.

Yang, V. 2000 Modeling of supercritical vaporization, mixing, and combustion processes in liquid-fueled propulsion systems. *Proceedings of the Combustion Institute* **28**, 925–942.